EXPERIMENTAL STUDY ON THE INFLUENCE OF STEAM PRESSURE DISTRIBUTION ON WOOD FIBER FEEDING

蒸汽压力分布对木纤维进给影响实验研究

Ao WANG [1], Guangwei CHEN [1], FaYi QU *[2], Yaoning YANG [1]
[1]Northeast Forestry University, College of Mechanical and Electrical Engineering, Harbin / China;
[2]Northeast Forestry University, Graduate School, Harbin / China.
DOI: https://doi.org/10.35633/inmateh-76-64

Keywords: *Heat mill; Grinding room; Saturated steam; Pressure distribution; Feed characteristics*

ABSTRACT

In this study, a non-invasive experimental method based on the shell temperature field was proposed to invert the internal steam pressure, aiming to investigate the distribution characteristics of saturated steam pressure within the mill chamber of the heat mill and its dynamic influence on the feed of wood fiber material feeding. The surface temperature field of the grinding chamber shell was measured by a high-precision infrared thermometer. Combined with the inverse heat conduction problem model and SteamTab software conversion, the cross-scale mapping relationship of "shell temperature-internal pressure" was constructed, and the pressure distribution cloud map was generated. The experimental materials consisted of mixed wood chips with a moisture content of 45±2%. After preheating and cooking at 160°C for 3 min, the chips were fed into the grinding chamber to analyze the coupling effect of the pressure field and the tooth shape parameters of the grinding disc. The results showed that the saturated steam pressure in the grinding chamber was significantly non-uniformly distributed along the radial direction, and the pressure gradient was mainly driven by the gradient change of the tooth shape parameters of the grinding disc. A solution to the problem of blocking backflow and excessive feed caused by non-uniform distribution of steam pressure was proposed in combination with the tooth profile parameters of the grinding plate.

摘要

本研究提出一种基于壳体温度场的非侵入式实验方法，通过反演磨室内部蒸汽压力，探究热磨机磨室内饱和蒸汽压力的分布特性及其对木质纤维原料进料的动态影响机制。采用高精度红外测温仪测量磨室壳体表面温度场，结合反热传导问题模型与 SteamTab 软件转换，构建"壳体温度-内部压力"的跨尺度映射关系，并生成压力分布云图。实验材料为含水率 45±2%的混合木片，经 160℃预热蒸煮 3 分钟后送入磨室，分析压力场与磨盘齿形参数的耦合效应。结果表明：磨室内饱和蒸汽压力沿径向呈显著非均匀分布，压力梯度主要受磨盘齿形参数的梯度变化驱动；结合磨盘齿廓参数特性，提出了解决蒸汽压力非均匀分布引发的堵塞回流与过量进料问题的技术方案。

INTRODUCTION

The hot mill is a key piece of equipment in the manufacturing of wood composite materials, particularly fiberboards *(Zhang et al., 2016*). Its operation relies on the synergistic effect of high-temperature saturated steam and mechanical refining to achieve the separation of wood fibers *(Wu et al., 2015*). During thermo-mechanical pulping, the spatial distribution of saturated steam pressure and temperature within the grinding chamber profoundly influences critical process parameters, including the degree of wood softening, fiber separation efficiency, and ultimately, the quality of the final products *(Xiong et al., 2014*).

Trairat Neimsuwan et al. (2008) focused on the effects of steam pressure on the performance of loblolly pine fibers during thermal refining. Their study revealed that higher steam pressure causes fiber surface damage, reducing moisture adsorption capacity and water activity but increasing crystallinity. In contrast, lower pressure maintains higher adsorption rates. *Fokko Schütt et al. (2011)* employed JMP software (SAS Institute) to design experiments, demonstrating that varying steam temperature and cooking duration during poplar wood steam pretreatment significantly alters fiber chemical composition. Based on this, they identified optimal cooking conditions.

Ao WANG, Postgraduates; GuangWei CHEN Assoc.Prof.; FaYi QU, Assistant Research Fellow; Yaoning YANG, Postgraduates.

Takasawa Ryosuke et al. (2011) investigated the impact of initial wood-chip moisture content and cooking time on the performance of medium-density fiberboard (MDF) manufactured from Acacia mangium. Their results indicated that high moisture content (90%) + short cooking (3–6 minutes) maximizes the comprehensive mechanical properties of Acacia mangium-based fiberboard.

While these studies emphasize steam's influence on fiber quality, production efficiency is equally critical in practice. This study thus targets the grinding chamber—the core component of thermal refiners—to examine how internal steam pressure distribution affects fiber feedstock feeding *(Liu et al., 2020*). However, the grinding chamber's harsh environment (high temperature/pressure, hermetic sealing, and complex geometry) impedes contact-based measurement of its internal steam pressure field. Consequently, the dynamic coupling mechanism between steam pressure distribution and fiber separation remains unclarified, severely limiting precise process control and optimization (*Wang et al., 2025*).

To address these limitations, a novel non-invasive experimental method is proposed to characterize saturated steam pressure distribution within the grinding chamber. The core innovation lies in deducing internal steam pressure from the shell's temperature field. Specifically: A high-precision infrared thermometer measures the shell surface temperature distribution. The Inverse Heat Conduction Problem (IHCP) method (*Min et al., 2022*) and SteamTab software (for saturated steam property conversion) analyze temperature data to establish a cross-scale mapping between the shell temperature field and internal steam pressure field. This approach enables the derivation and visualization of saturated steam pressure distribution.

Building on the inferred pressure distribution, this study further investigates the dynamic influence of this spatial pressure heterogeneity on the feeding behavior of fiber materials, particularly in relation to the geometric parameters of the grinding disc teeth. The main objectives are to:

- Quantitatively characterize the saturated steam pressure distribution within the operational grinding chamber.
- Systematically reveal the effect of this pressure field's spatial heterogeneity on fiber material feed dynamics.
- Propose targeted solutions to mitigate operational issues (e.g., backflow blockage, insufficient refining) arising from pressure non-uniformity.

The outcomes of this research have dual significance. Firstly, the developed non-invasive pressure inversion technique offers a new paradigm for analyzing multi-field coupling mechanisms within enclosed high-temperature, high-pressure industrial equipment like hot mills. Secondly, it enables online diagnosis of the internal pressure distribution through relatively simple shell temperature monitoring. This capability provides a direct scientific basis for optimizing production process parameters and refining grinding disc structural design *(Chen, 2012*), ultimately contributing to enhanced fiber separation uniformity and reduced unit energy consumption in the wood-based panel industry.

MATERIALS AND METHODS

Experiment equipment

The experiment was conducted in a hot mill at a wood-based panel plant in North China. The grinding disc had a diameter of 1.6 m, with a grinding disc gap ranging from 0.2 mm - 0.3 mm. A high-precision industrial infrared thermometer (Victory Instruments VC304F) was used to temperature measurements, with a measurement range of -40°C to 600°C, a temperature measurement frequency of 10 Hz, and employing 9-point laser positioning technology. The instrument was supplied by Suzhou Roebuck Measurement and Control Technology Co., Ltd., Suzhou, China.

Experiment materials

Poplar (60%) + pine (30%) + birch (10%) with a moisture content of 45±2% and a size of 15×15×5 mm) were preheated and cooked (160°C, 3 min).

Experimental methods and procedures

(1) Experiment purpose

To measure the temperature at the shell node of the grinding chamber and establish a cross-scale mapping model of the "shell temperature field–internal steam pressure field" by solving the inverse heat conduction problem, in order to investigate the distribution pattern of saturated steam pressure within the grinding chamber.

(2) Experimental operation flow

Preparation stage:

Observe the real-time monitoring and control panel of the hot mill to ensure the normal operation of the machine during the experiment; check whether the indoor temperature is within the allowable range of the temperature measuring instrument, and whether the reading of the temperature measuring instrument is normal.

Experimental stage:

Heat transfer from the interior to the exterior of the grinding chamber constitutes a multidimensional heat conduction process. During refining, frictional heat generation between the grinding disk and fibrous material occurs across the entire grinding disk surface, making this surface a distributed heat source.

Heat diffusion perpendicular to the normal direction is driven by local temperature gradients. However, in the planar direction, heat flow is supplemented and compensated by adjacent heat fluxes, resulting in minimal net lateral transfer. Therefore, when establishing a simplified thermal model for this system, primary attention can be directed to a one-dimensional heat conduction approximation perpendicular to the grinding disk surface (as illustrated in Fig. 1).

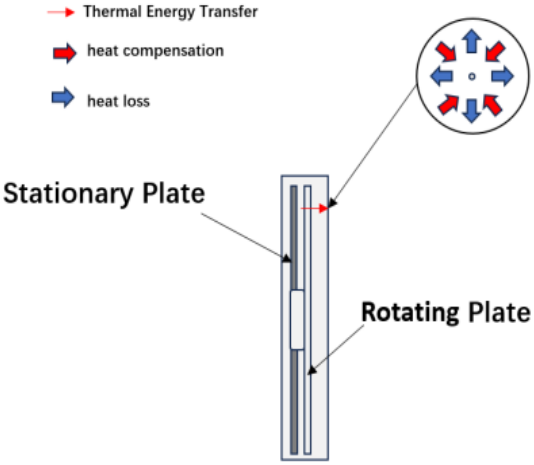

Fig. 1 - Grinding plate heat transfer analysis diagram

The pre-measurement points of the outer shell of the hot mill mode are divided. The outer circumference of the inlet is used as the initial measurement circumference, and the radius of the circumference is increased by 120 mm. Each measurement circumference is evenly distributed 12 points, a total of 84 measurement points, as shown in Fig. 2.

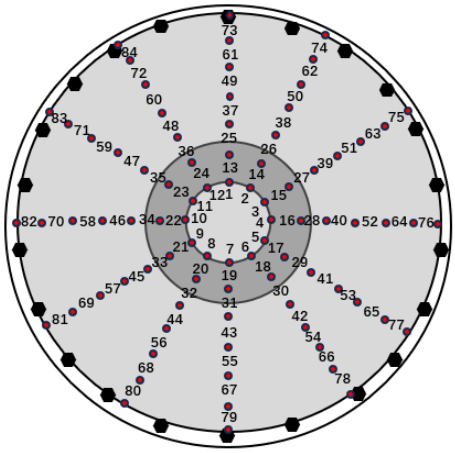

Fig. 2 - Experimental measurement point division

The temperatures at the above measurement points were measured using an industrial radiation thermometer positioned at 0.25 m from the measurement point (Fig. 3). Temperature data were recorded after the readings stabilized. Each measurement point was measured three times, and the average value was taken as the final recorded temperature.

Fig. 3 - Temperature measurement of outer shell of grinding chamber

The heat transfer from the interior of the grinding chamber to its shell is an extremely complex process. To simplify the problem and highlight the research focus *(Hua et al., 2015*), the following assumptions were made:

The shell of the hot mill grinding chamber has a uniform thickness.

The transient effect is neglected, and the heat conduction process is considered steady-state *(Chen et al., 2013)*.

Based on actual working conditions, the thermal conductivity of steam is treated as an average value.

The effects of friction and heat transfer between the fiber slurry and steam, as well as between the steam and the inner wall of the shell, are disregarded.

In the process of heat flux q transferring from the internal steam to the outer wall of the shell, two modes of heat transfer occur: (1) convection between the steam and the grinding disc of the hot mill, and (2) conduction from the grinding disc to the outer wall of the shell. These two heat transfer modes correspond to two kinds of thermal resistance, respectively, internal convective heat transfer thermal resistance - $Rconv=1/h_{in}A$ (h_{in} is the convective heat transfer coefficient between steam and inner wall, A is the heat transfer area), and wall thermal conductivity thermal resistance -d/kA (d is the thickness of wall and grinding disc, k is the thermal conductivity of grinding chamber wall).

Therefore, the total thermal resistance is as follows.

$$R_{\text{total}} = R_{\text{conv}} + R_{\text{cond}} = \frac{1}{h_{\text{in}} A} + \frac{d}{kA} \tag{1}$$

In steady state, the heat flux q satisfies.

$$q = \frac{T_{\text{steam}} - T_{\text{outer}}}{R_{\text{total}}} \tag{2}$$

where:

T_{steam} is the internal steam temperature corresponding to the measurement node;

T_{outer} is the experimental measurement node temperature.

Further combining the heat flux expressions $q=h_{in}（T_{steam}- T_{inner}）$ and $T_{inner} = T_{outer}+qd/k$ (T_{inner} is the temperature of the inner wall of the disc), the internal steam temperature corresponding to the measurement node can be obtained by combining Formula (1) and Formula (2):

$$T_{\text{steam}} = T_{\text{outer}} \left(1 + \frac{h_{\text{in}} d}{k}\right) + \frac{qd}{k} \tag{3}$$

RESULTS

The temperature data of the measuring points are recorded as shown in Table 1.

Table 1

Temperatures of measuring points of outer shell of grinding chamber (°C)

Number of rounds/serial	1	2	3	4	5	6	7	8	9	10	11	12
1	133.6	132.5	133.7	134.6	135.9	131.2	131.8	133.6	133.9	135.9	135.6	135.0
2	135.5	137.6	137.4	135.9	140.0	138.9	137.6	139.6	136.7	137.5	140.0	136.6
3	150.6	152.5	157.5	157.7	156.5	155.4	152.3	155.6	156.4	152.5	155.3	157.5
4	160.6	166.4	167.4	163.2	166.9	166.4	167.2	162.3	164.9	165.3	167.3	168.3
5	177.4	177.3	172.5	174.7	179.0	176.5	179.2	173.4	178.8	175.0	176.9	174.9
6	170.0	170.0	169.5	170.0	168.8	167.5	170.0	168.9	169.4	168.3	170.0	169.4
7	165.6	163.9	165.0	163.3	164.5	165.0	163.3	164.3	164.2	165.0	163.4	164.7

According to Eq.(3) and industrial saturated steam pressure-temperature conversion software SteamTab, the experimental data of internal saturated steam temperature and pressure corresponding to the measurement points of the outer shell of the grinding chamber of the hot mill are obtained (as shown in Table 2).

Table 2

The measurement point of the outer shell of the grinding chamber corresponds to the internal saturated steam temperature / pressure table (°C/MPa)

Temperature / Pressure serial number	number of rounds	1	2	3	4	5	6	7
1		226.8/2.64	229.6/2.78	250.7/4.03	264.8/5.07	288.3/7.26	277.9/6.22	271.8/5.66
2		225.4/2.57	232.5/2.93	253.4/4.21	272.9/5.76	288.2/7.25	277.9/6.22	269.3/5.45
3		227/2.65	232.3/2.92	260.44.73	274.2/5.88	281.46.56	277.2/6.15	270.8/5.58
4		228.2/2.71	230.2/2.81	260.7/4.75	274.2/5.37	284.5/6.87	277.9/6.22	268.5/5.38
5		230/2.81	235.8/3.11	259/4.62	273.6/5.82	290.5/7.50	276.26.06	270.1/5.52
6		223.5/2.48	234.4/3.03	257.4/4.50	272.9/5.76	287/7.13	274.4/5.90	270.8/5.58
7		224.3/2.52	232,5/2.93	253.1/4.19	267.1/5.86	290.8/7.53	277.9/6.22	268.5/5.38
8		224.3/2.64	235.8/3.08	257.7/4.52	267.1/5.26	282.6/6.68	276.4/6.08	269.9/5.50
9		227.2/2.66	231.2/2.86	258.9/4.61	270.7/5.57	290.2/7.47	277/6.14	269.8/5.49
10		230.2/2.81	232.3/2.92	253.4/4.21	271.3/5.62	284.9/6.91	275.5/6.00	270.8/5.58
11		229.6/2.78	235.8/3.11	257.3/4.49	274.1/5.87	287.6/7.19	277.9/6.22	268.6/5.39
12		228.8/2.74	231.2/2.86	260.4/4.73	275.5/6.00	284.8/6.90	277/6.14	270.5/5.55

The temperature data at the entrance of the fiber slurry in the center of the grinding disc (as shown in Fig. 4) were obtained by measuring the junction point between the feeding spiral section and the entrance of the fiber slurry (215°C).

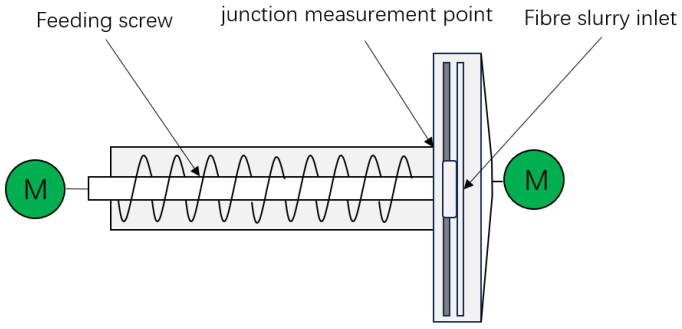

Fig. 4 - Schematic diagram of inlet end of fiber slurry

The afore-mentioned shell temperature and saturated steam pressure data of the mill chamber were imported into Origin software in the form of polar coordinates (ρ, θ, z). After matrix processing, the temperature distribution of the mill chamber shell and the internal saturated steam pressure distribution contour maps were generated, as shown in Fig. 5 and Fig. 6.

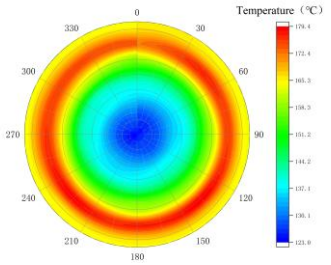

Fig. 5 - Temperature cloud diagram of grinding chamber shell

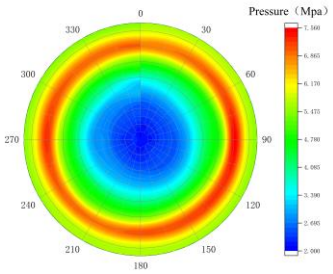

Fig. 6- The distribution of saturated steam pressure in the grinding chamber

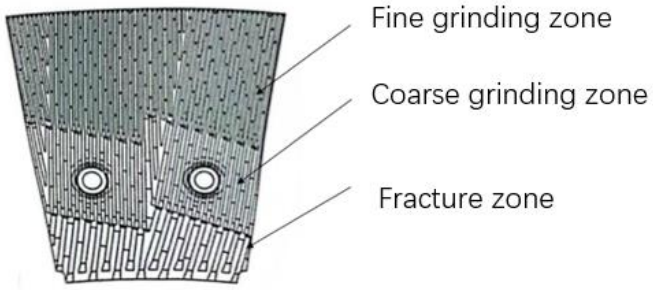

Fig. 7 - Grinding zone structure of grinding plate

Comparing the cloud image with the structure of the grinding area of the grinding disc (Fig. 7), the steam pressure shows a non-uniform distribution (first rising and then falling along the radial direction) in the crushing area, coarse grinding area and fine grinding area of the hot mill, which is due to the gradient change of the tooth shape parameters of the grinding disc (Table 3) and its synergistic regulation effect on the steam flow. The specific correlation mechanism is as follows:

Table 3

Grinding plate tooth profile parameters

Grinding plate partition	Tooth number	Tooth width [mm]	Tooth depth [mm]	Slot width [mm]	Tooth length [mm]	Tine angle [°]	Grinding gap [mm]
Fracture zone	48	8	10	21.2 ~36.3	95.1/259.2	56	0.30
Coarse grinding zone	312	4	9	5	18.9~148.0	39	0.25 ~0.27
Fine grinding zone	384	3	7	4	12.9~123.5	39	0.20

The tooth profile of the crushing zone is characterized by a wide tooth groove (the width of the groove is up to 21.2 ~ 36.3 mm, which is about 4 ~ 7 times that of the coarse grinding zone), the cross-sectional area of the steam channel (Ab = number of teeth × width of the groove × height of the tooth = 1.01 × 104 − 7.69 × 104mm^2) increases significantly, the flow resistance ($R \propto 1 / Ab^2$) decreases, and the large tooth inclination angle (φ = 56°) forms a divergent flow channel. The steam diffuses along the tooth surface, the pressure gradient is gentle (about 0.5 MPa/m), and the steam pressure has no obvious hindrance to the feed of the material. In this area, the centrifugal force plays a major role in the material. The overall material feed is stable and there is no risk of backflow.

When material reaches the primary grinding zone, the grinding gap narrows, subjecting coarse fibers to more intense and higher-frequency continuous dynamic loading. Concurrently, the presence of cross-bar teeth impedes rapid passage of steam and material within short timeframes. Consequently, rapid heat accumulation occurs within this confined space. At this time, the number of teeth increases to 312 (6.5 times of the crushing zone), the groove width decreases sharply to 5 mm, the cross-sectional area of the steam single channel decreases sharply (Ac = groove width × tooth height = 45mm^2), the cross-sectional area of the steam channel (Ab = tooth number × groove width × tooth height = 1.40 × 10^4), the flow resistance ($R \propto 1 / Ac^2$) is about 30 times higher than that of the crushing zone, and the pressure gradient reaches 3.6 MPa/m.

The saturated steam pressure reaches the peak at the junction of the coarse grinding zone and the fine grinding zone. The reason is that the material is changed from heat conduction to severe shear heating. According to the Clapeyron equation *(Liu et al., 2017*), the saturated vapor pressure has an exponential relationship with temperature ($P_{sat} \propto e - L/(RT)$, where L is the latent heat of vaporization).

Due to the centralized conversion of mechanical energy (from the kinetic energy of the disc rotor to thermal energy) and the location being at the junction where the cross-sectional area of the steam channel changes, material tends to accumulate in this region. This accumulation leads to a sharp local temperature increase, causing rapid vaporization of liquid water within the material. As a result, the steam generation rate in this area is significantly higher than in other regions. Under high pressure (8.5MPa), this can easily lead to material backflow along the radial direction of the grinding plate, ultimately causing blockages in material transmission.

When it reaches the fine grinding zone, the main component of the material is a small fiber bundle, and the way of heat generation is mainly concentrated in the high-speed crushing of the fiber bundle by the grinding teeth *(Hua et al., 2017*). The number of teeth in the fine grinding zone was further increased to 384 (23 % more than that in the coarse grinding zone), the gap between the grinding plates was reduced to 0.20 mm (80 % of that in the coarse grinding zone), and the cross-sectional area of the steam channel was reduced to 1.07 × 104 mm^2. However, due to the higher linear velocity in this region and the closer distance to the fiber outlet, the steam has enough centrifugal force to escape quickly from the outlet. When material reaches the primary grinding zone, the grinding gap narrows, subjecting coarse fibers to more intense and higher-frequency continuous dynamic loading. Concurrently, the presence of cross-bar teeth impedes rapid passage of steam and material within short timeframes. Consequently, rapid heat accumulation occurs within this confined space.

The sudden increase in tooth number density and the abrupt decrease in groove width in the rough grinding zone are the primary causes of the reverse pressure gradient. To prevent material blockage, the feed flow can be optimized by gradually increasing the tooth width and reducing the number of teeth in the rough grinding zone. To address the issue of overly fast feeding and insufficient fiber dissociation in the fine grinding zone, the number of grinding teeth in this area can be further increased to create multiple steam escape barriers, thereby slowing the steam escape rate. At the same time, the frequency of grinding tooth interaction with fiber is increased, promoting more thorough fiber dissociation.

CONCLUSIONS

The proposed non-invasive pressure inversion method overcomes the limitation of traditional invasive sensors, which cannot operate in harsh environments, and provides a new paradigm for multi-field coupling analysis of closed high-temperature and high-pressure equipment.

A cross-scale mapping model of “shell temperature field-internal steam pressure field” was established to analyze the distribution of saturated steam pressure in the grinding chamber and its influence on the feed of fiber materials. The results showed that the saturated steam pressure in the grinding chamber presented a non-uniform distribution along the radial direction of ”low pressure slow rise in the crushing zone (2.52-3.11 MPa)→ high pressure peak in the junction area between the coarse grinding zone and the fine grinding zone (6.00-7.53 MPa)→ rapid attenuation in the fine grinding zone (7.19-5.38 MPa)”. This phenomenon is due to the gradient change of the tooth shape parameters of the grinding disc. The fiber material is easy to cause the backflow blocking phenomenon in the coarse grinding area of the grinding plate, and the feed speed is too fast and the grinding is not sufficient in the fine grinding area. Solutions are proposed involving the use of progressive tooth width, reducing the number of teeth in the coarse grinding area, and increasing the number of teeth in the fine grinding area.

REFERENCES

[1] Chen G. (2012). *Model analysis and experimental study on the fiber separation mechanism of thermo-milling flakes (热磨法磨片纤维分离机理的模型分析与实验研究)* [D]. Northeast Forestry University.

[2] Chen K., Xu X., Ma K. (2013). Transient temperature field analysis of two-way gradient plate under heat flux / convective heat transfer boundary (热流密度/对流换热边界下双向梯度板的瞬态温度场分析) [J]. *Journal of Applied Mechanics*, Vol.30 (4), pp.563-568 + 648.

[3] Fokko S., Ju¨rgen P.,Bodo S.(2011). Optimization of steam pretreatment conditions for enzymatic hydrolysis of poplar wood *Eero [J]. *Holzforschung*, Vol. 65, pp. 453–459, 2011.

[4] Hua J., Chen G., Liu L. (2015). Numerical simulation of fiber flow in grinding flow field (纤维在研磨流场区域流动状况的数值模拟) [J]. *Journal of Northeast Forestry University*, Vol.43 (4), pp.113-118 + 130.

[5] Hua J., Lin X., Chen G. (2017). Establishment of fiber trajectory model in fine grinding zone and solution of grinding frequency (磨片精磨区纤维轨迹模型的建立及磨齿作用频数的求解) [J]. *Journal of Northeast Forestry University*, Vol.45 (04), pp.94-98.

[6] Liu F., Dong P., Wang G. (2020). New saturated vapor pressure and mass transfer coefficient test device (新型饱和蒸汽压及传质系数测试装置) [J]. *Laboratory research and exploration*, Vol, 39 (7), pp.71-73 + 83.

[7] Liu X., Lai H., Qu J. (2017) Discussion on the derivation of Clapeyron equation (关于 Clapeyron 方程推导的探讨) [J]. *Shandong Chemical Industry*, Vol.46 (16), pp.171 + 173.

[8] Min Ta, Han Y. (2022). Numerical solution of the inverse problem of initial conditions for two-dimensional heat conduction equations (二维热传导方程初始条件反问题的数值求解) [J]. *Mathematics*, Vol.42 (6), pp.513-522.

[9] Takasawa R., Shan N., Lin Z. (2019) The effect of initial moisture content and cooking time on the physical properties of MDF and cooking loss was studied (チップの初期含水率及び蒸煮時間が MDF 物性に及ぼす影響) [J]. *Journal of the Wood Society*, Vol. 65(1), pp.3-18.

[10] Trairat N., Siqun W., Xiaofei P.(2008). Effects of refining steam pressure on the properties of loblolly pine (Pinus taeda L.) fibers [J]. *Holzforschung*, Vol. 62, pp. 556-561.

[11] Wang C. (2025). Electrical Design of Grinding Disc Gap Control Based on Fiber Power Consumption (热磨机根据纤维功耗控制磨片间隙的电气设计) [J]. *China Wood-based Panels*, Vol.32 (2), pp.19-23.

[12] Wu J., Pan D., Huang L. (2015). Research, application and development of grinding plate of hot mill in China (我国热磨机磨片的研究应用及发展) [J]. *Casting technology*, Vol.36 (10), pp.2443-2447.

[13] Xiong J., Shen J., Song R. (2014). Factors affecting fiber quality during hot milling and solutions (热磨过程中影响纤维质量的因素及解决方法) [J]. *Forestry machinery and woodworking equipment*, Vol.42 (8), pp.38-39.

[14] Zhang S., Yan J., Hua J. (2016). Analysis of influencing factors of energy dissipation in fiber separation by hot milling (热磨法纤维分离能量耗散影响因素的分析) [J]. *Forestry industry*, Vol.43 (6), pp. 42-45.